

Article

# Validation of VIIRS AOD through a Comparison with a Sun Photometer and MODIS AODs over Wuhan

Wei Wang<sup>1</sup>, Feiyue Mao<sup>1,2,3,\*</sup>, Zengxin Pan<sup>1</sup>, Lin Du<sup>1,4</sup> and Wei Gong<sup>1,3,5</sup>

<sup>1</sup> State Key Laboratory of Information Engineering in Surveying, Mapping and Remote Sensing (LIESMARS), Wuhan University, Wuhan 430079, China; wangweicn@whu.edu.cn (W.W.); pzx@whu.edu.cn (Z.P.); linyufocus@foxmail.com (L.D.); weigong@whu.edu.cn (W.G.)

<sup>2</sup> School of Remote Sensing and Information Engineering, Wuhan University, Wuhan 430079, China

<sup>3</sup> Collaborative Innovation Center for Geospatial Technology, Wuhan 430079, China

<sup>4</sup> School of Physics and Technology, Wuhan University, 299, Bayi Road, Wuhan 430071, China

<sup>5</sup> Hubei Collaborative Innovation Center for High-Efficiency Utilization of Solar Energy, Wuhan 430068, China

\* Correspondence: maofeiyue@whu.edu.cn

Academic Editors: Yang Liu, Jun Wang, Omar Torres, Richard Müller and Prasad S. Thenkabail

Received: 22 February 2017; Accepted: 21 April 2017; Published: 25 April 2017

**Abstract:** Visible Infrared Imaging Radiometer Suite (VIIRS) is a next-generation polar-orbiting operational environmental sensor with a capability for global aerosol observations. A comprehensive validation of VIIRS products is significant for improving product quality, assessing environment quality for human life, and studying regional climate change. In this study, three-year (from 1 January 2014 to 31 December 2016) records of VIIRS Intermediate Product (IP) data and Moderate Resolution Imaging Spectroradiometer (MODIS) retrievals on aerosol optical depth (AOD) at 550 nm were evaluated by comparing them to ground sun photometer measurements over Wuhan. Results indicated that VIIRS IP retrievals were underestimated by 5% for the city. A comparison of VIIRS IP retrievals and ground sun photometer measurements showed a lower  $R^2$  of 0.55 (0.79 for Terra-MODIS and 0.76 for Aqua-MODIS), with only 52% of retrievals falling within the expected error range established by MODIS over land (i.e.,  $\pm(0.05 + 0.15AOD)$ ). Bias analyses with different Ångström exponents (AE) demonstrated that land aerosol model selection of the VIIRS retrieval over Wuhan was appropriate. However, the larger standard deviations (i.e., uncertainty) of VIIRS AODs than MODIS AODs could be attributed to the less robust retrieval algorithm. Monthly variations displayed largely underestimated AODs of VIIRS in winter, which could be caused by a large positive bias in surface reflectance estimation due to the sparse vegetation and greater surface brightness of Wuhan in this season. The spatial distribution of VIIRS and MODIS AOD observations revealed that the VIIRS IP AODs over high-pollution areas ( $AOD > 0.8$ ) with sparse vegetation were underestimated by more than 20% in Wuhan, and 40% in several regions. Analysis of several clear rural areas ( $AOD < 0.2$ ) with native vegetation indicated an overestimation of about 20% in the northeastern region of the city. These findings showed that the VIIRS IP AOD at 550 nm can provide a solid dataset with a high resolution (750 m) for quantitative scientific investigations and environmental monitoring over Wuhan. However, the performance of dark target algorithms in VIIRS was associated with aerosol types and ground vegetation conditions.

**Keywords:** aerosol; VIIRS; MODIS; sun photometer; AERONET

## 1. Introduction

Atmospheric aerosols such as those from biomass burning, dust minerals, volcanic ash, smoke, sea salt, and particulate pollution, are emitted from various natural and anthropogenic activities [1,2]. Atmospheric aerosols significantly influence the radiation budget of the Earth by affecting the

lifetime and microphysical properties of clouds, as well as precipitation rates and tropospheric photochemistry; therefore, they are significant in climate change studies [3–5]. However, aerosol sources, transport, and sinks possess a relatively short lifetime of one to two weeks in the atmosphere, and this characteristic restricts the understanding of their chemical and physical properties, as well as their spatiotemporal distribution characteristics [6,7]. A global network of ground-based sun photometers, such as the aerosol robotic network (AERONET) [8], provides regular measurements of aerosol optical properties, such as aerosol optical depth (AOD), at high temporal and spectral resolutions to better understand aerosol distributions in the atmosphere. However, these measurements are limited over space. This spatial limitation is addressed by satellite remote sensing, which provides systematic near-real-time AOD observations at low to high spatial resolutions [2,9,10]. Satellite remote sensing is recognized as an ideal method for monitoring the spatiotemporal distribution of AOD at regional and global scales. Aerosol retrieval algorithms are developed for global distributions of AOD by using different satellite sensors, such as the advanced very-high-resolution radiometer (AVHRR) [11], sea-viewing wide field of view sensor [12], total ozone-mapping spectroradiometer [13], ozone-monitoring instrument [14], multi-angle imaging spectroradiometer [15], moderate-resolution imaging spectroradiometer (MODIS) [2,9,10], and Visible Infrared Imaging Radiometer Suite (VIIRS) [16,17].

In October 2011, VIIRS was launched aboard the Suomi National Polar-orbiting Partnership (S-NPP) satellite; VIIRS is a new generation of operational satellite sensors for the characterization aerosol [16]. The VIIRS instrument is designed using many of the features of the National Aeronautics and Space Administration's Earth-Observing System MODIS, which has produced near-real-time aerosol data products for over a dozen years [18,19]. Given the similarity in the design of the two instruments, VIIRS is expected to produce aerosol products that are similar in scope and capability as those of MODIS [16]. The VIIRS aerosol calibration/validation team continuously monitors, evaluates, and improves the performance of VIIRS aerosol retrievals [16,17]. However, the accuracy and consistency of retrieving aerosol products via VIIRS remain worse than that of MODIS [16], due to uncertainties from cloud screening, radiance calibration, and aerosol optical property modeling. Thus, further studies that find uncertainty sources or reduce uncertainties are significant for the successful accomplishment of the VIIRS mission.

With the rapid growth of the Chinese economy in recent years, air pollution has reached a critical level, resulting in the uncertain aerosol climate on Earth due to rapid urbanization and increased industrial activity [20]. However, spatial and temporal variations in aerosols in China are poorly understood because of the sparse network of observations, or limited satellite observations with high precision and resolution [21]. VIIRS is expected to serve as a powerful tool for large-scale aerosol observations with a high spatial resolution (750 m). Therefore, the performance of VIIRS should be compared and validated against that of ground- and space-based sensors before VIIRS aerosol products are applied in scientific research in China. The VIIRS AOD Intermediate Product (IP) was evaluated with ground-measured AOD from over 12 selected AERONET sites and compared with MODIS aerosol data over China in 2013 [22]. The spatiotemporal variations in AOD retrieved from VIIRS in eastern China was also investigated [23]. Emerging aerosol products from VIIRS, MODIS (Collection 6), and Geostationary Ocean Color Imager in East Asia were evaluated in 2012 and 2013 by using ground AOD observations from AERONET and handheld sun photometers [24]. However, these upfront validation studies were conducted in the coastal areas of China. VIIRS AOD validation with AERONET is limited spatially, because most regions in Asia are empty, especially in central China [16]. Furthermore, the VIIRS data of urban areas exhibit more discrepancy than the ground measurements [23]. Therefore, additional validation study in urban region in central China is necessary to determine the performance of VIIRS.

The objective of this study is to investigate the performances of VIIRS and MODIS in the AOD retrievals over Wuhan, China by comparing data recorder in three years (from 1 January 2014 to 31 December 2016) with those from a ground-based sun photometer. The qualities of VIIRS IP and

MODIS Terra/Aqua AODs are evaluated in Section 4.1. The monthly AOD characteristics are studied with VIIRS IP, MODIS, and sun photometer data in Section 4.2. The spatial distribution of VIIRS and MODIS AOD observations is shown in Section 4.3. The reasons for the AOD difference between the three tools over Wuhan are also discussed.

## 2. Study Area and Datasets

### 2.1. Study Area

The rapid economic growth and population expansion in China in the past three decades has resulted in drastic increases in energy consumption, which has significantly increased AOD over a large part of China [22]. Wuhan is the largest city in central China, with a dense population and heavy industrialization on the Yangtze River Basin (indicated by the white point in Figure 1). Wuhan experiences a typical north subtropical humid monsoon climate, with an annual average temperature of 15.8 °C to 17.5 °C and an annual average rainfall of 1050 mm to 2000 mm [25,26]. Most areas in Wuhan are 50 m above sea level. Figure 1 shows the location and terrain of Wuhan.

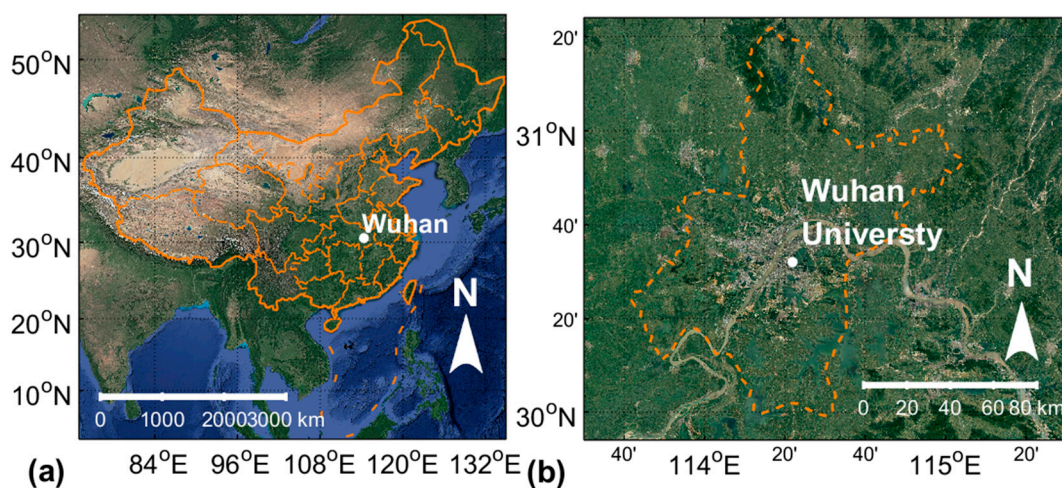


**Figure 1.** (a) Location of Wuhan in China and (b) location of the sun photometers at Wuhan University (white point).

### 2.2. Datasets

#### 2.2.1. Sun Photometer Data

A Cimel sun photometer, CE-318, was placed and operated on top of the LIESMARS building (30°32'N, 114°21'E, and 30 m above sea level) at Wuhan University (WHU), Wuhan, Hubei Province, China, in July 2007 (Figure 1b). The CE-318 sun photometer manufactured by Cimel Electronique Company (France), is a multi-channel, automatic, sun-and-sky-scanning radiometer that measures direct solar irradiance and sky radiance. The instrument performs direct spectral solar radiation measurements within a 1.2 full field of view every 15 min at eight normal bands of 340, 380, 440, 500, 675, 870, 940, and 1020 nm [27]. The total uncertainty of AOD is approximately 0.01 to 0.02 [28]. The observations from August 2007 can be used to investigate the aerosol optical properties in central China. Several problems occurred in the equipment from April to November 2013. CE-318 is annually calibrated with China Meteorological Administration Aerosol Remote Sensing Network (CARSNET) reference instruments to ensure data accuracy and reliability; the detailed calibration procedures are described in [29]. The AOD data were calculated using ASTPwin software (Cimel Co., Ltd., Paris, Phalsbourg, France) for level 1.5 AOD. The retrieval method is found in [30].

### 2.2.2. VIIRS Data

VIIRS is one of the key environmental remote-sensing instruments onboard the Suomi NPP satellite. This instrument is a scanning radiometer that can extend and improve upon the heritage of AVHRR and MODIS [16]. VIIRS aerosol retrieval is performed at the pixel level and produces aerosol products with a spatial resolution of 0.75 km [31]. The product of this process, known as IP, is then aggregated and designated as an Environmental Data Record (EDR) reported at 6 km ( $8 \times 8$  pixels) resolution at nadir [16]. In this work, we evaluated VIIRS AOD550s at IP level. AOD550s are the most important aerosol parameters used by models and other community-wide applications. Quality assurance is applied at IP levels, with the resulting flags indicating the confidence of the retrievals as described in detail in [16]. For the current study, a three-year (from 1 January 2014 to 31 December 2016) dataset of AOD from VIIRS IP with quality flag = 0 (good), was analyzed to evaluate the performance of VIIRS in Wuhan.

### 2.2.3. MODIS Data

The detailed retrieval principle of the MODIS dark target (DT) algorithm over land can be found in [9,18,32]. The DT AOD product at 3 km is developed from spectral reflectance using a similar look-up-table and inversion based on the ratio of visible and shortwave infrared as the 10-km product [19,33]. MODIS AOD products with high resolutions (3 km) are expected to address aerosol gradients and pollution sources missed at 10 km. The quality of MODIS aerosol retrievals generally depends on the accuracy of the surface reflectance and the aerosol model, and over- or underestimation under clear and polluted conditions are normally caused by an error in these two factors [34,35]. The MODIS C6 DT AOD product significantly and systematically overestimates the AOD of Asian cities [35,36]. In this study, MOD04 and MYD04 C006 DT aerosol products were obtained over Wuhan, and only the highest-quality-flag (QF = 3) AOD observations were considered for analysis. To distinguish the different MODIS DT C006 datasets in this study, we marked them as “MOD04\_3K” and “MYD04\_3K” for Terra-MODIS and Aqua-MODIS AOD at 3 km, respectively.

## 3. Comparison and Verification of Methods

According to suggestions from other research groups [16,22,24], data matching was performed with the following rules. First, the mean AOD was averaged when at least 20% of the pixels fell within the sampling box. Second, observed AODs with a standard deviation greater than 0.5 were excluded, whereas satellite data (covering an area of  $20 \text{ km} \times 20 \text{ km}$ ) near each WHU site were selected to reduce validation uncertainty due to the atmospheric variability imposed by atmospheric motion. Sun photometer data acquired within 30 min of the satellite overpass times were collected from 2014 to 2016. The data provided by a sun photometer did not have the 550 nm channel, and AODs at 550 nm were calculated by linear interpolation at a log scale from two measurements with adjacent wavelengths [16]. To show how accurately the satellite AOD matched the evaluation datasets, the following metrics were applied. A regression technique was used to estimate the slope and intercept of the datasets, and the uncertainty in the aerosol algorithms was evaluated using the expected error (EE, Equation (1)) over land, the relative mean bias (RMB, Equation (2)) that indicates the average overestimation ( $\text{RMB} > 1.0$ ) or underestimation ( $\text{RMB} < 1.0$ ) for the retrieval AODs, the root-mean-square error (RMSE, Equation (3)), the mean absolute error (MAE, Equation (4)), and the Pearson correlation coefficient ( $R$ ).

$$EE = \pm(0.05 + 0.15AOD_{ground}) \quad (1)$$

The MODIS AOD expected errors (EE) were  $\pm(0.05 + 0.15AOD)$  over land [16,19,33].

$$RMB = \frac{\overline{AOD}_{(satellite)}}{\overline{AOD}_{(ground)}} \quad (2)$$

$$RMSE = \sqrt{\frac{1}{n} \sum_{i=1}^n \left( AOD_{(satellite)i} - AOD_{(ground)i} \right)^2} \quad (3)$$

$$MAE = \frac{1}{n} \sum_{i=1}^n \left| AOD_{(satellite)i} - AOD_{(ground)i} \right| \quad (4)$$

## 4. Results and Analysis

### 4.1. Validation of VIIRS IP and MODIS C006 AOD

Figure 2a–c show the comparisons of satellite AOD retrievals with ground observations over the Wuhan region. The total times that the satellite passed over the WHU site within 20 km and 30 min for VIIRS, Terra, and Aqua were about 1092, 1084, and 1097, respectively; by contrast, the numbers of valid matchups with the ground sun photometer were 284, 242, and 202, respectively. The relatively few valid matchups over the three-year period were caused by cloud cover and sun photometer maintenance.

VIIRS IP indicated a linear regression slope of 0.69 and a positive intercept of 0.18 on average against ground observations. The comparison of VIIRS IP retrievals with the ground sun photometer measurements showed a low  $R^2$  of 0.55, with RMB being equal to 0.95, and only 52% of retrievals falling within EE (Figure 2a). RMB = 0.95 suggested that VIIRS IP underestimated (5%) the retrieval AODs. The scatter plot illustrates that the IP retrievals varied substantially, especially given high AOD values. A global study from 23 January 2013 to 31 December 2014 revealed similarly underestimated results with sample numbers (20269), accuracy (0.0415), precision (0.155), uncertainty (0.160), slope (0.730), intercept (0.089), and  $R^2$  (0.549) in the land AOD IP versus AERONET [17]. However, this result was inconsistent with a previous validation study, in which 32% of VIIRS IP retrievals fell into the EE, with a slightly low  $R^2$  of 0.63, and a relatively large positive bias (0.25) in Beijing within 3 km around AERONET [24]. The different aerosol types may have caused this difference between Beijing and Wuhan. Beijing is easily affected by downwind dust (weakly absorbing and coarse mode aerosol) from large northern deserts, but the aerosol model over this region in VIIRS has too much absorption [2]. Therefore, weakly absorbing aerosol model may be considered when dust is prominent [19].

MODIS C006 3 km products showed a large RMB at 1.13 for Terra-MODIS and 1.07 for Aqua-MODIS, which suggests a mean overestimation of 13% for MOD04\_3K and 7% for MYD04\_3K. Of the Terra-MODIS C6 3 km retrievals and the Aqua-MODIS C6 3 km retrievals, 66% and 71% fell within EE, respectively. MODIS with high spatial retrievals (3 km) was highly correlated with the ground AOD with  $R^2$  of 0.79 and 0.76, for MOD04\_3K and MYD04\_3K, respectively. The linear regressions of MODIS retrievals and ground AOD were close to the 1:1 line. MODIS valid matchups were smaller than those of VIIRS over the same sun photometer sites, but the MODIS retrievals were better correlated with ground measurements than the VIIRS data (Figure 2 and Table 1). A previous global validation study of the 3 km MODIS AOD data reported similar retrieval errors ( $R^2$  for Aqua and Terra were 0.68 and 0.85 respectively, and the intercepts for Aqua and Terra were 0.22 and 0.30 respectively) in urban areas [33]. Moreover, a recent study reported that MODIS C6 3 km product produced a higher bias (0.21 for Aqua and 0.29 for Terra) in a comparison with AERONET in Beijing, as well as the lowest within EE (44% for Aqua and 25% for Terra) [24]. The higher bias may be attributed to the lower average area (within  $9 \times 9 \text{ km}^2$ ) around AERONET. Similar results were reported by other evaluation studies on MODIS C6 3 km aerosol retrieval algorithms over bright urban surfaces of Beijing during low and high aerosol loadings [32]. Similarly, a recent evaluation study for the MYD04\_3K over Asian countries with severe pollution showed that a large, significant overestimation was observed at urban sites dominated by coarse aerosols, including Beijing, Karachi, and Osaka, at 93.20%, 94.55%, and 75.76% of observations above the EE, respectively [2]. These results are similar to the C6 DT algorithm at 10 km, which was also found to be overestimated over cities in China and Pakistan against AERONET [1,37]. These overestimations in MODIS C006 3 km products may be attributed to a large underestimation in surface reflectance, because these study regions are

highly urbanized with bright surfaces, which posed a challenge to the DT algorithm [2,24]. In addition, mixing aerosols with non-absorbing and absorbing fine mode aerosols over urban regions causes over-prediction for absorption, which results in AOD overestimation.

Comparisons over the Wuhan region showed more MODIS retrievals falling within EE and larger  $R^2$  than VIIRS in the WHU site. From preliminary global verification over land from 23 January 2013 to 1 September 2013 by the VIIRS aerosol validation team, compared with AERONET, VIIRS retrievals showed comparable accuracy ( $-0.009$  versus  $-0.005$ ), larger uncertainty (0.130 versus 0.106), and lower correlation ( $R$ : 0.773 versus 0.886) than MODIS [16]. The fine-resolution aerosol products showed greater noise than the low-resolution products, which may explain the better performance of MODIS.

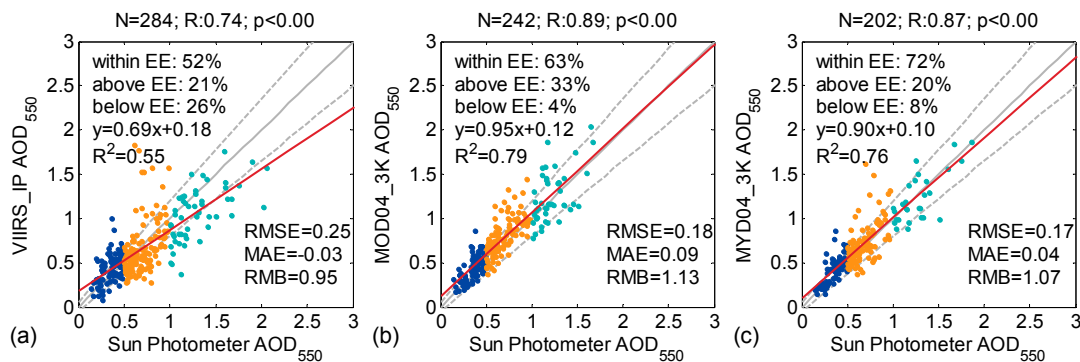


**Figure 2.** Validation of Visible Infrared Imaging Radiometer Suite (VIIRS) (a), and Moderate Resolution Imaging Spectroradiometer (MODIS) C006 aerosol optical depth (AOD) (b,c) observations (QF = high) against the Wuhan sun photometer AOD at 550 nm measurements from 2014 to 2016. The red line is the regression line, the gray solid line is the 1:1 line, and the gray dashed lines are the expected errors (EE) envelopes.

Figure 3 shows the box plots indicating the difference between satellite AOD retrievals and ground observations. The box plot in Figure 3a presents the VIIRS IP retrievals underestimated (overestimated) AOD under  $AOD > 1.0$  ( $AOD < 0.3$ ). The AOD, ranging between 0.3 and 1.0, agreed well with the ground sun photometer observations. This finding was inconsistent with a previous validation study, wherein the VIIRS product tended to overestimate AOD at low ( $AOD < 0.3$ ) and high ( $AOD > 1.0$ ) AOD values in East Asia [24]. Figure 3b,c present box plots showing the difference between MODIS AOD retrievals and ground observations. The bias between MODIS and sun photometer AODs was small across the entire AOD range, and was within EE when the AOD was above 0.3. However, several overestimations in AOD retrievals were also observed when AOD was low ( $AOD < 0.3$ ) (Figure 3b). This finding was consistent with a previous global evaluation study, in which MODIS C6 3 km products tended to overestimate AOD [33]. The results indicated that MODIS has better accuracy than VIIRS in terms of AOD retrievals over Wuhan. The statistical results of the temporal comparisons between satellite retrievals and ground AOD measurements at 550 nm over Wuhan from 2014 to 2016 are shown in Table 1.

Figure 3d–f plot the differences between VIIRS (MODIS) and sun photometer AOD against the AE measured by sun photometer from 440 nm to 870 nm, which depicts the relationship between AOD biases and aerosol particle sizes [16,17]. AE can reflect aerosol particle sizes and their corresponding aerosol model selections. The present study found that average positive biases (the middle circle in each figure) of MODIS AOD in Figure 3e,f are larger than VIIRS IP retrievals (Figure 3d) when AE is less than 0.6. The aerosol types in Wuhan may be influenced by downwind dust (low AE) transported by prevailing north winds from the large northern deserts at winter monsoon period [26]. The smaller biases of VIIRS IP AODs confirmed the use of a proper aerosol model in VIIRS. However, the larger standard deviations (i.e., uncertainty in AODs) of VIIRS AODs could be attributed to the less robust retrieval algorithm. The biases of VIIRS IP AODs arose with increases in AE (Figure 3d), indicating

more negative biases for fine particles, especially where  $AE > 1.3$ , whereas MODIS AOD showed less biases against sun photometer AODs. The negative bias at  $AE > 1.3$  influenced most of the systematic underestimation of VIIRS IP AODs (Figure 2a), and the underestimation is explained in the next subsection analyses about monthly variations. The fine mode aerosols with strong absorption and large AE over Wuhan often have a dominant function due to automobile exhaust and the use of coal for domestic cooking, heating, and industrial processes [25]. Moreover, most matchups over a broad range of particle sizes (0.6–1.3 of AE), show smaller retrieval bias but larger uncertainty than MODIS. The results demonstrate that the aerosol model selection of the VIIRS retrieval is appropriate in this evaluation region, but the robustness of the retrieval algorithm needs improvement.

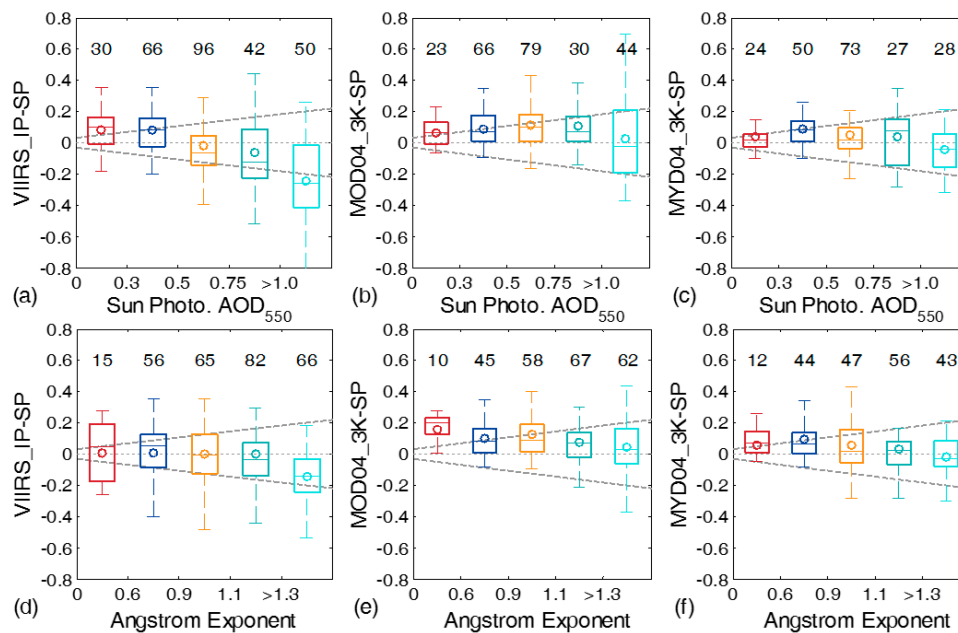


**Figure 3.** Box plots of AOD<sub>550</sub> differences (satellite—sun photometer) versus sun photometer AOD at 550 nm (a–c) and Ångström Exponent (d–f) over the Wuhan region. The number above each box refers to the corresponding statistical collocations. The  $y = 0$  line (zero error) is shown as a fine dashed line, and the boundary lines of the expected error are depicted as gray coarse dashed lines. The properties and statistics representing each box whisker include the following: the solid lines in each box indicate the 25th and 75th percentiles of the AOD error, the whiskers are the maximum and minimum of the AOD error, the middle line is the median value of the AOD error, and the middle circle is the mean value of the AOD error.

**Table 1.** Statistics of the comparisons between satellite retrievals and ground AOD measurements at 550 nm over Wuhan from 2014 to 2016.

	N	$R^2$	Slope	Intercept	% Above/Within/Below EE
VIIRS IP 0.75 km	284	0.55	0.69	0.18	21/52/26
Terra MODIS C6 3 km	242	0.79	0.95	0.12	33/63/4
Aqua MODIS C6 3 km	202	0.76	0.90	0.10	20/72/8

#### 4.2. Monthly Variations in VIIRS, MODIS, and Sun Photometer AOD Observations

The monthly AOD observations derived from VIIRS, MODIS, and the sun photometer over the WHU sites during the study period were analyzed (Figure 4). The annual average AODs were  $0.66 \pm 0.33$  for 10:30 local time (LT) (Figure 4a) and  $0.63 \pm 0.33$  for 13:30 LT (Figure 4b). Compared to the previous study, the result was smaller than the multi-year average of AOD at 550 nm measured by the sun photometer at  $1.05 \pm 0.66$  in urban Wuhan [38]. The bias attributes to the average AOD of the

latter were from a whole day. Moreover, the result was similar to those of suburban and background stations in the literature; for example, yearly mean AODs are equal to 0.82 at 500 nm at Xianghe [39], about 0.6 at Shenyang [40] and about  $0.50 \pm 0.06$  in the Bohai Rim economic zone [41].

The monthly AODs varied with a bimodal curve. The peak values at 10:30 LT appeared in April and August (Figure 4a), and two peak values at 13:30 LT appeared in spring and autumn. The seasonal cycles of both the VIIRS IP, MODIS derived and sun photometer-measured AODs showed the same trends, which are consistent with previous studies, such as the work of [23,42]. The monthly mean AODs were related to the Asian dust and anthropogenic emission patterns in March–May, but they were modified by precipitation in June–July. A large amount of straw is burned in farmlands from nearby provinces during the harvest seasons (summer and autumn), thereby leading to the frequent haze conditions in recent years [43]. Moreover, increasing industrial and human activities, such as cement processing, smelting, coal combustion, and automobile emissions, generally lead to severe air pollution [25]. Climatologically, Wuhan is located in the East Asian monsoon area. The Meiyu period in the Yangtze River Delta during mid-June and late July [44] corresponds to the low AODs during the rainy period from June to July.

Overall, the VIIRS and MODIS AODs presented the same trend, but were over- or underestimated in different months against the ground-measured results in the WHU site. The comparison of monthly Terra-MODIS and sun photometer AODs measured at about 10:30 LT indicated a significant overestimation by MOD04\_3k, especially from March to June (Figure 4a). Although the Aqua-MODIS product tended to overestimate AOD from February to June, the data agreed well with ground observations from June to November (Figure 4b). The MODIS overestimation may have been related to the difference in surface reflection caused by surface vegetation in various months. The VIIRS IP products and ground sun photometer measurements indicated similar monthly mean AOD observations over the Wuhan sites from June to November, and larger underestimations in winter (January, February, and December). Liu et al. pointed out that the seasonal variability in the biases relatively depended on the seasonally variation of vegetation growth and senescence [16]. Therefore, the larger underestimated AODs in winter could be attributed to the large positive bias in surface reflectance estimation, due to sparse vegetation with larger surface brightness in Wuhan during this season.

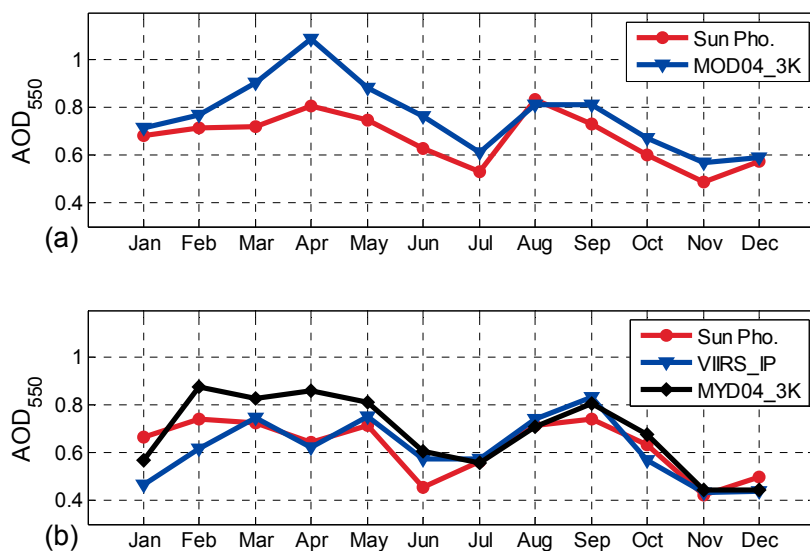


**Figure 4.** Monthly variations using different collocated satellite remote-sensing AODs and ground sun photometer measurements (AOD at 550 nm) over Wuhan from 1 January 2014 to 31 December 2016: (a) 10:30 local time (LT) and (b) 13:30 LT.

### 4.3. Spatial Distribution of VIIRS and MODIS AOD Observations

Figure 5 shows the three-year mean spatial distribution of VIIRS IP, MOD04 3 km, and MYD04 3 km (QF = high) over the Wuhan region and its surroundings used for comparisons with VIIRS and MODIS AOD products. Similar aerosol load distributions are found in Figure 5a–c. The aerosol loads around the Yangtze River and at the city center of Wuhan were significantly higher than nearby northeast rural areas, possibly because of intense anthropogenic activity and industrialized pollution. The comparison results showed that VIIRS and MODIS could realize AOD retrievals over Wuhan, but VIIRS was able to describe aerosol distribution and variability in greater detail at a higher spatial resolution (750 m) than the current MOD04 AOD products, which could produce 3 km spatial resolution can under both low and high aerosol loads (Figure 5a). Although the three collections showed a similar spatial distribution pattern, the underestimated AOD retrieved by VIIRS over the city center of Wuhan was significant compared to MODIS AOD.

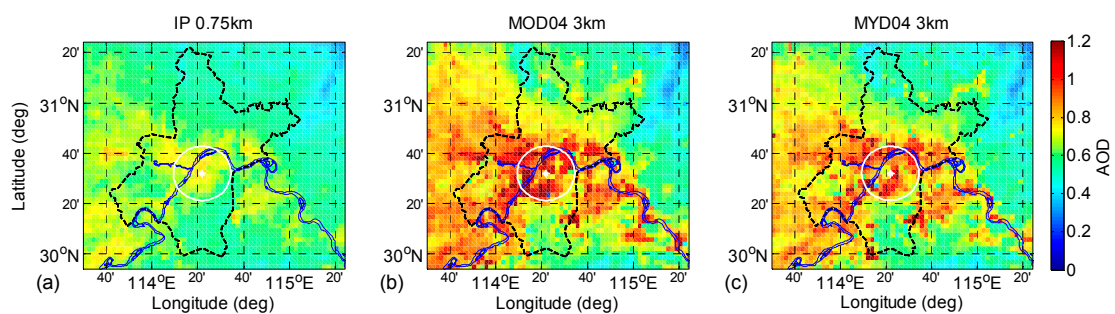


**Figure 5.** Mean AOD spatial distribution of (a) VIIRS IP 0.75 km, (b) MOD04 3 km, and (c) MYD04 3 km from 2014 to 2016. The white point denotes the Wuhan University (WHU) site; the white circle represents the city center of Wuhan and the average area for satellite data.

As stated in Section 4.1, the MODIS AOD retrievals had higher accuracy than VIIRS (Figure 2 and Table 1); therefore, the spatial distribution of VIIRS IP AOD could be evaluated by MODIS AOD retrievals. VIIRS IP AODs at 0.75 km resolution were resampled to 3 km spatial resolution, similar to the MODIS AOD retrievals. The AOD difference (%) in Figure 6 is defined as “ $100 \times (\text{VIIRS} - \text{MODIS}) / \text{MODIS}$ ”, which describes the average difference between VIIRS IP and MODIS retrievals. The greater differences between VIIRS IP and Terra-MODIS (Figure 6a) than those between VIIRS IP and Aqua-MODIS (Figure 6b) may contribute to Terra-MODIS overpassing Wuhan at approximately 10:30 LT, and VIIRS IP at approximately 13:30 LT. Unlike Terra-MODIS, Aqua-MODIS is quasi-synchronous with VIIRS.

The VIIRS IP AODs over the high-pollution areas ( $\text{AOD} > 0.8$ ) with sparse vegetation were underestimated by more than 20% and 40% in Wuhan and several regions, respectively. By contrast, several clear areas ( $\text{AOD} < 0.2$ ) presented an overestimation of about 20% in the northeastern region, as depicted in Figure 6. The smallest AOD differences (−10% to 10%) were observed in the transition regions ( $0.2 < \text{AOD} < 0.8$ ). These conclusions are similar to those of the VIIRS and ground measurement comparisons in Section 4.1. As discussed in [16], the biases between the VIIRS and MODIS AODs are potentially related to surface conditions such as surface brightness and vegetation coverage, because the aerosol retrieval algorithm does not work well in urban areas with bright reflective regions [19,23]. The biases are due to the limitations of the DT algorithm over sparse vegetated surfaces, because Wuhan is dominated by built-up and bare land surfaces (Figure 1), and the retrieval quality depends on the surface reflectance and aerosol model schemes used in the look-up table. These results suggest that the aerosol model and surface reflectance applied in the DT algorithm should be treated separately according to different aerosol types and land cover characteristics. These analyses could help reduce the uncertainty in AOD products using the DT retrieval algorithm of VIIRS and MODIS. Overall, the DT algorithm in VIIRS still needs improvement and modifications to achieve good accuracy, similar to that of MODIS AOD retrievals.

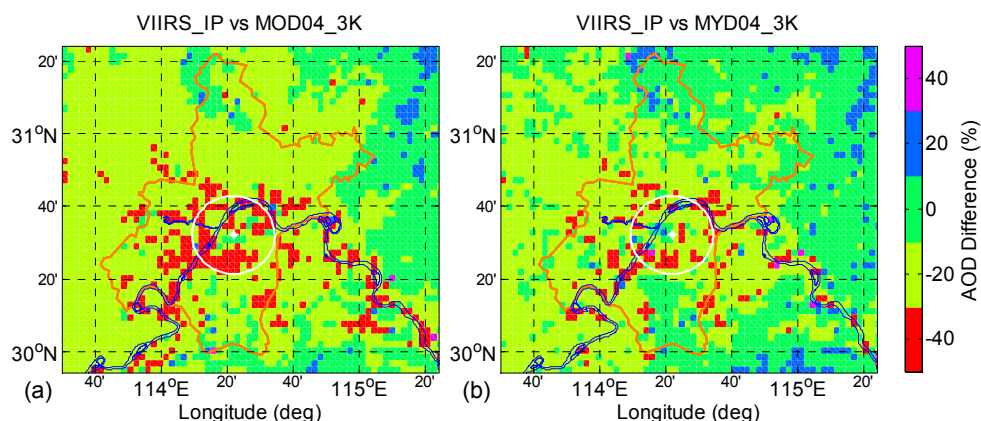


**Figure 6.** Mean spatial distribution of the AOD difference from 2014 to 2016: (a) VIIRS IP vs. MOD04 3 km and (b) VIIRS IP vs. MYD04 3 km. The negative and positive signs indicate under- and overestimations, respectively.

## 5. Conclusions

The VIIRS sensor, which is a next-generation polar-orbiting operational environmental sensor with a capability for global aerosol observations, provided the multi-year global aerosol data used in this study. In this work, VIIRS and MODIS high-quality AODs at 550 nm over Wuhan were validated against ground sun photometer measurements. The comparison spanned from 1 January 2014 to 31 December 2016. Compared with the ground sun photometer measurements over Wuhan, the VIIRS AOD IP exhibited an underestimation by 5% for cities. On the contrary, the MODIS C006 AOD retrievals were significantly overestimated over the Wuhan sites, with mean overestimations of 13% and 7% for Terra and Aqua, respectively. The evaluation and comparison of the results showed that the VIIRS IP retrievals and ground sun photometer measurements had a low  $R^2$  of 0.55, with only 52% of retrievals falling within the expected error range established by MODIS over land. The MODIS AODs indicated higher correlations (0.79 for Terra and 0.76 for Aqua) with the ground sun photometer measurements and lower RMSEs (0.18 for Terra and 0.17 for Aqua) and MAE values (0.09 for Terra and 0.04 for Aqua) than the VIIRS IP AOD products. Bias analyses demonstrated an appropriate aerosol model selection of the VIIRS retrieval over Wuhan, but the larger standard deviations (i.e., uncertainty) of VIIRS AODs than that of MODIS AODs were attributed to the less robust retrieval algorithm. Monthly variations displayed larger underestimated AODs of VIIRS in winter, which was attributed to the large positive bias in surface reflectance estimation, due to sparse vegetation and the larger surface brightness of Wuhan in this season. The spatial distribution of VIIRS and MODIS AOD observation revealed that the VIIRS IP AODs over the high-pollution areas ( $AOD > 0.8$ ) with sparse vegetation were underestimated by more than 20% and 40% in Wuhan and several regions, respectively. By contrast, several clear areas ( $AOD < 0.2$ ) indicated an overestimation of about 20% in the northeastern region. In summary, the VIIRS IP AOD at 550 nm can provide a solid dataset with a high resolution (750 m) for quantitative scientific investigations and environmental monitoring over Wuhan. However, the performance of dark target algorithm in VIIRS is associated with aerosol types and ground vegetation conditions, and it needs to be improved and modified to achieve good accuracy, similar to that of MODIS AOD retrievals. This study and its results are indispensable for achieving a better, more accurate evaluation of VIIRS AODs with high spatial resolution in urban cities, which will play an important role in the assessment of environment quality for human life, and research on regional climate change.

**Acknowledgments:** This research is supported by the National Key Research and Development Program of China (2016YFC0200900), the National Natural Science Foundation of China (41627804), the Program for Innovative Research Team in University of the Ministry of Education of China (IRT1278), the National Science Foundation of Hubei Province (2015CFA002), and the China Postdoctoral Science Foundation (2016T90731).

**Author Contributions:** The work presented here was conducted in collaboration with all authors. Feiyue Mao, Zengxin Pan, Lin Du, Wei Gong and Wei Wang defined the research theme. All authors performed the experiments. This manuscript was written by Wei Wang. Feiyue Mao and Zengxin Pan checked the experimental results. All authors agreed to the submission of the manuscript.

**Conflicts of Interest:** The authors declare no conflict of interest.

## References

1. Bilal, M.; Nichol, J.E.; Nazeer, M. Validation of Aqua-MODIS C051 and C006 operational aerosol products using AERONET measurements over Pakistan. *IEEE J. Sel. Top. Appl. Earth Obs. Remote Sens.* **2016**, *9*, 2074–2080. [[CrossRef](#)]
2. Nichol, J.; Bilal, M. Validation of MODIS 3 km resolution aerosol optical depth retrievals over Asia. *Remote Sens.* **2016**, *8*, 328. [[CrossRef](#)]
3. Twomey, S. Aerosols, clouds and radiation. *Atmos. Environ. Part A Gen. Top.* **1991**, *25*, 2435–2442. [[CrossRef](#)]
4. Pan, Z.; Gong, W.; Mao, F.; Li, J.; Wang, W.; Li, C.; Min, Q. Macrophysical and optical properties of clouds over east Asia measured by CALIPSO. *J. Geophys. Res. Atmos.* **2015**, *120*. [[CrossRef](#)]
5. Pan, Z.; Mao, F.; Gong, W.; Wang, W.; Yang, J. Observation of clouds macrophysical characteristics in China by CALIPSO. *J. Appl. Remote Sens.* **2016**, *10*, 036028. [[CrossRef](#)]
6. He, Q.; Li, C.; Mao, J.; Lau, A.; Li, P. A study on the aerosol extinction-to-backscatter ratio with combination of micro-pulse lidar and MODIS over Hong Kong. *Atmos. Chem. Phys.* **2006**, *6*, 3243–3256. [[CrossRef](#)]
7. Logan, T.; Xi, B.; Dong, X.; Li, Z.; Cribb, M. Classification and investigation of Asian aerosol absorptive properties. *Atmos. Chem. Phys.* **2013**, *13*, 2253–2265. [[CrossRef](#)]
8. Holben, B.; Eck, T.; Slutsker, I.; Tanre, D.; Buis, J.; Setzer, A.; Vermote, E.; Reagan, J.; Kaufman, Y.; Nakajima, T. Aeronet—A federated instrument network and data archive for aerosol characterization. *Remote Sens. Environ.* **1998**, *66*, 1–16. [[CrossRef](#)]
9. Remer, L.A.; Kaufman, Y.; Tanré, D.; Mattoo, S.; Chu, D.; Martins, J.V.; Li, R.-R.; Ichoku, C.; Levy, R.; Kleidman, R. The MODIS aerosol algorithm, products, and validation. *J. Atmos. Sci.* **2005**, *62*, 947–973. [[CrossRef](#)]
10. Kittaka, C.; Winker, D.; Vaughan, M.; Omar, A.; Remer, L. Intercomparison of column aerosol optical depths from CALIPSO and MODIS-Aqua. *Atmos. Meas. Tech.* **2011**, *4*, 131–141. [[CrossRef](#)]
11. Hauser, A.; Oesch, D.; Foppa, N.; Wunderle, S. NOAA AVHRR derived aerosol optical depth over land. *J. Geophys. Res. Atmos.* **2005**, *110*. [[CrossRef](#)]
12. Sayer, A.M.; Hsu, N.C.; Bettenhausen, C.; Jeong, M.J. Global and regional evaluation of over-land spectral aerosol optical depth retrievals from SeaWiFS. *Atmos. Meas. Tech.* **2012**, *5*, 2169–2220. [[CrossRef](#)]
13. Torres, O.; Bhartia, P.K.; Herman, J.R.; Sinyuk, A.; Ginoux, P.; Holben, B. A long-term record of aerosol optical depth from toms observations and comparison to AERONET measurements. *J. Atmos. Sci.* **2002**, *59*, 398–413. [[CrossRef](#)]
14. Torres, O.; Tanskanen, A.; Veihelmann, B.; Ahn, C.; Braak, R.; Bhartia, P.K.; Veeffkind, P.; Levelt, P. Aerosols and surface uv products from ozone monitoring instrument observations: An overview. *J. Geophys. Res. Atmos.* **2007**, *112*, 1–14. [[CrossRef](#)]
15. Kahn, R.A.; Gaitley, B.J.; Garay, M.J.; Diner, D.J.; Eck, T.F.; Smirnov, A.; Holben, B.N. Multiangle imaging spectroradiometer global aerosol product assessment by comparison with the aerosol robotic network. *J. Geophys. Res. Atmos.* **2010**, *115*, D23209. [[CrossRef](#)]
16. Liu, H.; Remer, L.A.; Huang, J.; Huang, H.-C.; Kondragunta, S.; Laszlo, I.; Oo, M.; Jackson, J.M. Preliminary evaluation of s-NPP VIIRS aerosol optical thickness. *J. Geophys. Res. Atmos.* **2014**, *119*, 3942–3962. [[CrossRef](#)]
17. Huang, J.; Kondragunta, S.; Laszlo, I.; Liu, H.; Remer, L.A.; Zhang, H.; Superczynski, S.; Ciren, P.; Holben, B.N.; Petrenko, M. Validation and expected error estimation of Suomi-NPP VIIRS aerosol optical thickness and angström exponent with AERONET. *J. Geophys. Res. Atmos.* **2016**, *121*, 7139–7160. [[CrossRef](#)]

18. Levy, R.C.; Remer, L.A.; Mattoo, S.; Vermote, E.F.; Kaufman, Y.J. Second-generation operational algorithm: Retrieval of aerosol properties over land from inversion of moderate resolution imaging spectroradiometer spectral reflectance. *J. Geophys. Res. Atmos.* **2007**, *112*. [[CrossRef](#)]
19. Levy, R.C.; Mattoo, S.; Munchak, L.A.; Remer, L.A.; Sayer, A.M.; Patadia, F.; Hsu, N.C. The collection 6 MODIS aerosol products over land and ocean. *Atmos. Meas. Tech.* **2013**, *6*, 2989–3034. [[CrossRef](#)]
20. Zhang, Y.-L.; Cao, F. Fine particulate matter (PM<sub>2.5</sub>) in China at a city level. *Sci. Rep.* **2015**, *5*. [[CrossRef](#)] [[PubMed](#)]
21. Guo, J.-P.; Zhang, X.-Y.; Wu, Y.-R.; Zhaxi, Y.; Che, H.-Z.; La, B.; Wang, W.; Li, X.-W. Spatio-temporal variation trends of satellite-based aerosol optical depth in China during 1980–2008. *Atmos. Environ.* **2011**, *45*, 6802–6811. [[CrossRef](#)]
22. Meng, F.; Cao, C.; Shao, X. Spatio-temporal variability of Suomi-NPP VIIRS-derived aerosol optical thickness over China in 2013. *Remote Sens. Environ.* **2015**, *163*, 61–69. [[CrossRef](#)]
23. Meng, F.; Xin, J.; Cao, C.; Shao, X.; Shan, B.; Xiao, Q. Seasonal variations in aerosol optical thickness over eastern China determined from VIIRS data and ground measurements. *Int. J. Remote Sens.* **2016**, *37*, 1868–1880. [[CrossRef](#)]
24. Xiao, Q.; Zhang, H.; Choi, M.; Li, S.; Kondragunta, S.; Kim, J.; Holben, B.; Levy, R.C.; Liu, Y. Evaluation of VIIRS, GOCI, and MODIS collection 6 AOD retrievals against ground sunphotometer observations over east Asia. *Atmos. Chem. Phys.* **2016**, *16*, 20709–20741. [[CrossRef](#)]
25. Wang, L.; Gong, W.; Xia, X.; Zhu, J.; Li, J.; Zhu, Z. Long-term observations of aerosol optical properties at wuhan, an urban site in central China. *Atmos. Environ.* **2015**, *101*, 94–102. [[CrossRef](#)]
26. Wang, W.; Gong, W.; Mao, F.; Pan, Z.; Liu, B. Measurement and study of lidar ratio by using a raman lidar in central China. *Int. J. Environ. Res. Public Health* **2016**, *13*, 508. [[CrossRef](#)] [[PubMed](#)]
27. Dubovik, O.; Smirnov, A.; Holben, B.N.; King, M.D.; Kaufman, Y.J.; Eck, T.F.; Slutsker, I. Accuracy assessments of aerosol optical properties retrieved from aerosol robotic network (AERONET) sun and sky radiance measurements. *J. Geophys. Res. Atmos.* **2000**, *105*, 9791–9806. [[CrossRef](#)]
28. Eck, T.F.; Holben, B.N.; Reid, J.S.; Dubovik, O.; Smirnov, A.; O'Neill, N.T.; Slutsker, I.; Kinne, S. Wavelength dependence of the optical depth of biomass burning, urban, and desert dust aerosols. *J. Geophys. Res. Atmos.* **1999**, *104*, 31333–31349. [[CrossRef](#)]
29. Tao, R.; Che, H.; Chen, Q.; Wang, Y.; Sun, J.; Zhang, X.; Lu, S.; Guo, J.; Wang, H.; Zhang, X. Development of an integrating sphere calibration method for cimel sunphotometers in China aerosol remote sensing network. *Particuology* **2014**, *13*, 88–99. [[CrossRef](#)]
30. Smirnov, A.; Holben, B.N.; Eck, T.F.; Dubovik, O.; Slutsker, I. Cloud-screening and quality control algorithms for the AERONET database. *Remote Sens. Environ.* **2000**, *73*, 337–349. [[CrossRef](#)]
31. Jackson, J.M.; Liu, H.; Laszlo, I.; Kondragunta, S.; Remer, L.A.; Huang, J.; Huang, H.-C. Suomi-NPP VIIRS aerosol algorithms and data products. *J. Geophys. Res. Atmos.* **2013**, *118*, 12673–12689. [[CrossRef](#)]
32. Bilal, M.; Nichol, J.E. Evaluation of MODIS aerosol retrieval algorithms over the Beijing-Tianjin-Hebei region during low to very high pollution events. *J. Geophys. Res. Atmos.* **2015**, *120*, 7941–7957. [[CrossRef](#)]
33. Remer, L.A.; Mattoo, S.; Levy, R.C.; Munchak, L. MODIS 3 km aerosol product: Algorithm and global perspective. *Atmos. Meas. Tech.* **2013**, *6*, 69–112. [[CrossRef](#)]
34. Chu, D.; Kaufman, Y.; Ichoku, C.; Remer, L.; Tanré, D.; Holben, B. Validation of MODIS aerosol optical depth retrieval over land. *Geophys. Res. Lett.* **2002**, *29*, 8007. [[CrossRef](#)]
35. He, Q.; Li, C.; Tang, X.; Li, H.; Geng, F.; Wu, Y. Validation of MODIS derived aerosol optical depth over the Yangtze river delta in China. *Remote Sens. Environ.* **2010**, *114*, 1649–1661. [[CrossRef](#)]
36. Tao, M.; Chen, L.; Wang, Z.; Tao, J.; Che, H.; Wang, X.; Wang, Y. Comparison and evaluation of the MODIS collection 6 aerosol data in China. *J. Geophys. Res. Atmos.* **2015**, *120*, 6992–7005. [[CrossRef](#)]
37. Remer, L.A.; Kleidman, R.G.; Levy, R.C.; Kaufman, Y.J.; Tanré, D.; Mattoo, S.; Martins, J.V.; Ichoku, C.; Koren, I.; Yu, H.; et al. Global aerosol climatology from the MODIS satellite sensors. *J. Geophys. Res. Atmos.* **2008**, *113*. [[CrossRef](#)]
38. Wang, W.; Gong, W.; Mao, F.; Zhang, J. Long-term measurement for low-tropospheric water vapor and aerosol by raman lidar in Wuhan. *Atmosphere* **2015**, *6*, 521–533. [[CrossRef](#)]
39. Li, Z.; Xia, X.; Cribb, M.; Mi, W.; Holben, B.; Wang, P.; Chen, H.; Tsay, S.-C.; Eck, T.F.; Zhao, F.; et al. Aerosol optical properties and their radiative effects in northern China. *J. Geophys. Res. Atmos.* **2007**, *112*, 321–341. [[CrossRef](#)]

40. Che, H.; Zhao, H.; Wu, Y.; Xia, X.; Zhu, J.; Wang, H.; Wang, Y.; Sun, J.; Yu, J.; Zhang, X.; et al. Analyses of aerosol optical properties and direct radiative forcing over urban and industrial regions in northeast China. *Meteorol. Atmos. Phys.* **2015**, *127*, 345–354. [[CrossRef](#)]
41. Xin, J.; Wang, L.; Wang, Y.; Li, Z.; Wang, P. Trends in aerosol optical properties over the Bohai rim in northeast China from 2004 to 2010. *Atmos. Environ.* **2011**, *45*, 6317–6325. [[CrossRef](#)]
42. Meng, F.; Cao, C.Y.; Shao, X.; Shi, Y.G. Spatial and temporal variation of visible infrared imaging radiometer suite (VIIRS)-derived aerosol optical thickness over Shandong, China. *Int. J. Remote Sens.* **2014**, *35*, 6023–6034. [[CrossRef](#)]
43. Xia, X.; Zong, X.; Sun, L. Exceptionally active agricultural fire season in mid-eastern China in June 2012 and its impact on the atmospheric environment. *J. Geophys. Res. Atmos.* **2013**, *118*, 9889–9900. [[CrossRef](#)]
44. Luo, Y.; Zheng, X.; Zhao, T.; Chen, J. A climatology of aerosol optical depth over China from recent 10 years of MODIS remote sensing data. *Int. J. Climatol.* **2014**, *34*, 863–870. [[CrossRef](#)]



© 2017 by the authors. Licensee MDPI, Basel, Switzerland. This article is an open access article distributed under the terms and conditions of the Creative Commons Attribution (CC BY) license (<http://creativecommons.org/licenses/by/4.0/>).